Acta Biomaterialia 64 (2017) 15–28

Contents lists available at ScienceDirect

Acta Biomaterialia

journal homepage: www.elsevier.com/locate/actabiomat

Full length article

Viscoelastic properties of α-keratin fibers in hair

Yang Yu [a], Wen Yang [b,c], Marc André Meyers [a,b,*]

[a] Department of NanoEngineering, University of California, San Diego, La Jolla, CA, United States
[b] Materials Science and Engineering Program, University of California, San Diego, La Jolla, CA, United States
[c] Department of Materials, Eidgenössische Technische Hochschule Zürich, Zürich 8093, Switzerland

ARTICLE INFO

Article history:
Received 4 May 2017
Received in revised form 30 July 2017
Accepted 12 September 2017
Available online 14 September 2017

Keywords:
α-Keratin fibers
Viscoelasticity
Strain-rate sensitivity
Stress relaxation
Creep

ABSTRACT

Considerable viscoelasticity and strain-rate sensitivity are a characteristic of α-keratin fibers, which can be considered a biopolymer. The understanding of viscoelasticity is an important part of the knowledge of the overall mechanical properties of these biological materials. Here, horse and human hairs are examined to analyze the sources of this response. The dynamic mechanical response of α-keratin fibers over a range of frequencies and temperatures is analyzed using a dynamic mechanical analyzer. The α-keratin fibers behave more elastically at higher frequencies while they become more viscous at higher temperatures. A glass transition temperature of ~55 °C is identified. The stress relaxation behavior of α-keratin fibers at two strains, 0.02 and 0.25, is established and fit to a constitutive equation based on the Maxwell-Wiechert model. The constitutive equation is further compared to the experimental results within the elastic region and a good agreement is obtained. The two relaxation constants, 14 s and 359 s for horse hair and 11 s and 207 s for human hair, are related to two hierarchical levels of relaxation: the amorphous matrix-intermediate filament interfaces, for the short term, and the cellular components for the long term. Results of the creep test also provide important knowledge on the uncoiling and phase transformation of the α-helical structure as hair is uniaxially stretched. SEM results show that horse hair has a rougher surface morphology and damaged cuticles. It also exhibits a lower strain-rate sensitivity of 0.05 compared to that of 0.11 for human hair. After the horse and human hairs are chemically treated and the disulfide bonds are cleaved, they exhibit a similar strain-rate sensitivity of ~0.05. FTIR results confirms that the human hair is more sensitive to the –S–S– cleavage, resulting in an increase of cysteic acid content. Therefore, the disulfide bonds in the matrix are experimentally identified as one source of the strain-rate sensitivity and viscoelasticity in α-keratin fibers.

Statement of significance

Hair has outstanding mechanical strength which is equivalent to metals on a density-normalized basis. It possesses, in addition to the strength, a large ductility that is enabled by either the unfolding of the alpha helices and/or the transformation of these helices to beta sheets. We identify the deformation and failure mechanisms and connect them to the hierarchical structure, with emphasis on the significant viscoelasticity of these unique biological materials.

1. Introduction

Fibrous keratin fibers, such as wool [1–3], human hair [4–6], and whale baleen [7] have been widely studied due to their superior mechanical strength [8,9]. These fibers usually have a protective and defensive function for animal bodies and yet yield some unnoticed properties. For example, wool has a high tensile strength of 200–260 MPa, yielding a specific tensile strength (normalized to density equal to 1.3 Mgm^{-3}) of 150–200 MPa/Mgm^{-3}, which is comparable to some stainless steels (~250 MPa/Mgm^{-3}). Additionally, wool and human hair usually have a large extensibility, with a breaking strain of more than 40%. Therefore, researchers have been interested in the mechanical properties and morphologies of keratin fibers [10,11], hoping to be able to mimic these materials.

Every hair fiber has a hierarchical structure [12], as shown in Fig. 1. A typical human hair fiber has a diameter of 50–100 μm and the outermost layer composed of cuticles that ensure the integrity of the fibers. These cuticle scales, which are 0.3–0.5 μm

* Corresponding author at: Department of NanoEngineering, University of California, San Diego, La Jolla, CA, United States.
E-mail address: mameyers@eng.ucsd.edu (M. André Meyers).

https://doi.org/10.1016/j.actbio.2017.09.012
1742-7061/

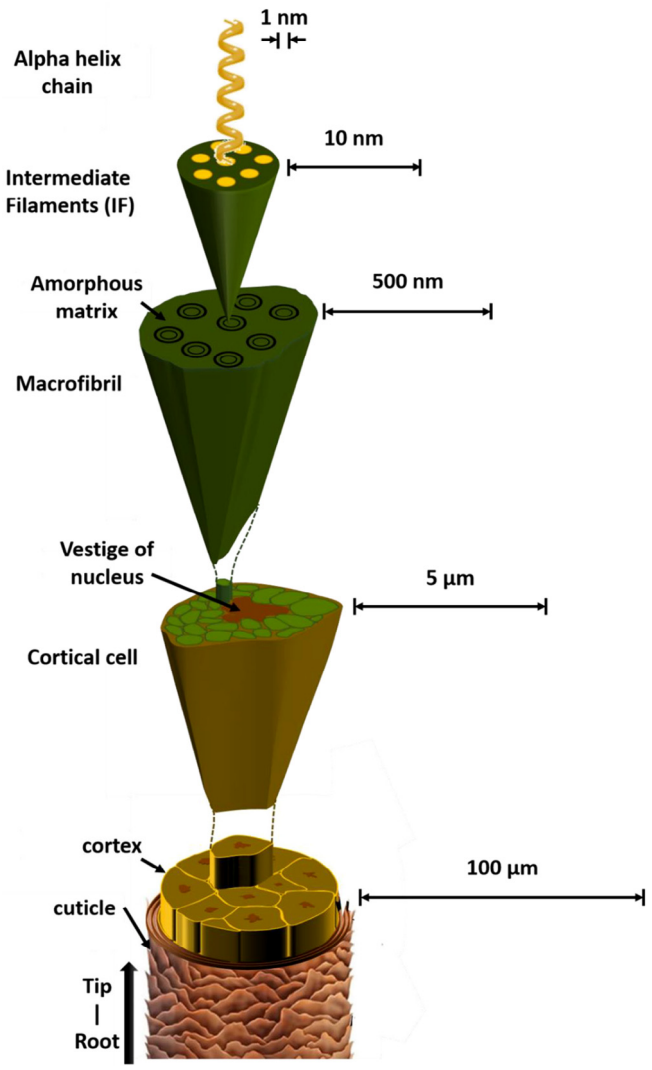

Fig. 1. Schematic drawing of the hierarchical structure in a human hair fiber. Human hair has a range of diameters of 17–180 μm while horse tail hair has a larger (75–280 μm) diameters. These values represent the broadest range which is much larger than the specimens studied herein.

thick and 40–60 μm long, also have a layered structure [6]. The inner section, cortex, is composed of cortical cells that are 100 μm long. Moreover, each cortical cell is comprised of macrofibrils with ~0.2–0.4 μm diameter; these macrofibrils are further composed of intermediate filaments (IFs) (7.5 nm in diameter) embedded in an amorphous matrix. These intermediate filaments are made from α-helical polypeptide chains. Due to this hierarchical structure and different components of crystalline fibrils (intermediate filaments) and amorphous matrix, human hair exhibits strain-rate sensitivity [13] and viscoelasticity [14,15]. Stress relaxation experiments on both human [16] and camel hair [17] reveal that the stress decreases as a function of time as the hair fiber is strained to specific values. In the meanwhile, age and ethnicity may also play important roles in the relaxation rate [18].

At the beginning of the tensile tests, these α-helical chains experience a reversible bond angle rearrangement in the elastic region (0 ~ 0.02–0.05 strain). Following this region, the structure will undergo either an uncoiling of the helical chains or a phase transformation from α-helix to parallel β-sheets within the transformation region (~0.05 to ~0.25 strain). Since there is no or little resistance in these processes, the stress-strain curve in this region exhibits a very slow increase in stress. Once the strain is larger than ~0.25, the curve goes into the post-transformation region and the unchanged α-keratin chains and possibly-formed β-keratin will be further stretched until breakage. Research has shown that, depending on the experimental conditions, the crystal structure in hair may experience an uncoiling behavior [19] or phase transformation [2,20]. Therefore, the behavior of such phase transformation has to be factored with analysis of viscoelasticity of α-keratin fibers. Moreover, dynamic mechanical characterization, which has been applied to analyze various biological materials [21–23], can also provide important information on the viscoelasticity of α-keratin fibers.

Apart from the well-studied wool and human hair, horse hair is also a hard α-keratin fiber that has attracted interest during the past decade. Researchers have shown that horse hair has a crystalline structure that is the same as human hair [19,24]. Horse tail hair has been widely used in a lot of applications, such as brushes and bows of violins, due to its superior mechanical properties. It is considered very strong but also flexible. Its response is highly influenced by factors such as diet [25] and climate such as humidity [26] and temperature [27], in a similar manner to other keratin fibers. Different from human hair that is regularly taken care of, horse hair is usually subjected to weathering and rough handling. Therefore, it is thought that by studying and comparing the different mechanical properties among these two alike hair samples, we will be able to gain insights in the sources of viscoelasticity and the strain-rate sensitivity in the keratin fibers.

One of the unique properties of keratin fibers is their viscoelasticity. Stress relaxation studies by Barnes et al. [15] showed that the relaxation modulus changes according to different strains and time duration. Robinson et al. [16] showed that differences in the mechanical properties and different thiol content along the hair fibers are found. The viscoelasticity in the human hair further yields many consequences. Among these, significant strain-rate sensitivity has been observed in our previous study [8]. On the other hand, the Young's modulus remains unchanged across all strain rates, indicating that it is an inherent material property. It is suggested that, at small extensions, stress relaxation mainly comes from deformation of the peptide bonds and chemical groups; as the strain further increases, the amorphous matrix, which is regarded as an elastomer in the Chapman model to explain the tensile properties of keratin fibers [2], mainly contributes to the viscoelasticity.

The goal of the investigation whose results are presented here was to elucidate the mechanisms responsible for viscoelasticity in hair and to identify critical differences between human and horse hair.

2. Materials and methods

2.1. Sample preparation

Human hair was acquired exclusively from an East-Asian female in her early 30s. This is to guarantee the uniformity of the mechanical properties obtained in our experiments and excludes the influences of age and ethnicity as previously observed [18,28–30]. The hair had only experienced regular rinsing and shampooing. No additional treatments such as permanent waving and dyeing had been previously done on these hair specimens. The hair was directly tested without further moistening or shampooing.

Horse hair was collected from the tail of a 16-year-old Arabian gelding. The horse hair was briefly rinsed to remove the dirt and further kept under room condition for over 24 h to remove the moisture. The average length of each hair fiber is about 30 cm. To prevent the influence of property differences from the root and

tip ends [16], these fibers are then cut at ~2 cm from both ends. Approximately 3 cm-long sections were made from the long fibers. The two ends of the 3 cm-long sections are further glued between sand papers to prevent slipping during tensile tests, leaving a 1 cm-long hair specimen in between for tensile tests. During tensile tests, the two sand papers were pulled to prevent slipping of the hair specimens in the grips during tensile tests.

Wild boar, javelina, bear, Asian elephant, and giraffe hair were procured and also studied to establish the effect of diameter on the strength and elastic modulus. The Asian elephant and giraffe hair were obtained from QinLing Safari Park (Xi'an, China), whereas the boar, javelina, and bear hair were procured from a local hunter. These hairs were tested using the same methodology as the human and horse hair.

Specimens tested in water were pre-soaked for 24 h to reach full saturation. The two ends were mounted into epoxy to prevent splitting during soaking. The human hair specimens tested at 40 and 60 °C were heated in an environmental chamber for at least 20 min before testing and maintained at those temperatures during experiments. The room temperature testing was conducted at 20 °C; the room humidity was 50%. The drying of the hair removes only the humidity up to the ambient value.

2.2. Mechanical testing

An Instron 3342 with a 500 N load cell was used to test the hair specimens at strain rates of 10^{-4}, 10^{-3}, 10^{-2}, 10^{-1}, and 10^{0} s^{-1} at room temperature and humidity. In the stress relaxation tests, both horse and human hair specimens were each stretched to 0.02 and 0.25 strains, at a strain rate of 10^{-3} s^{-1}. These two strain levels (0.02 and 0.25 strains) were chosen to show different behaviors, corresponding to the elastic and transformation regions. The loading times were, respectively, 20 and 250 s. As the strains were held, the stresses were monitored for a time over 1000s. For the creep test, hair specimens were first stretched within the elastic region (0.02) at a strain rate of 10^{-3} s^{-1} until the stress reached to 90 MPa for horse hair and 100 MPa for human hair. The strains were then recorded until the hair specimens broke.

2.3. Dynamic mechanical analysis (DMA)

The dynamic mechanical behavior of α-keratin fibers was analyzed using a DMA 800 Dynamic Mechanical Analyzer (Perkin Elmer). The hair specimens were clamped tightly in the chamber and the temperature was increased at a rate of 5 °C min^{-1} until 30 °C. The specimens underwent an oscillated tensile test within the elastic region as the total strain did not exceed 0.01 by increasing the frequency from 0.1 to 2.4 Hz. The storage modulus and tangent delta (equal to the ratio of loss to storage modulus) were recorded at each frequency. Hair specimens were tested within the same strain, 0.01, at a set frequency of 0.75 Hz while the temperature inside the chamber increased from 30 °C to 110 °C at a rate of 5 °C min^{-1}. The dynamic properties of hair at different frequencies and temperatures were thus obtained to help understand the viscoelasticity of α-keratin fibers.

2.4. Chemical treatment process

The disulfide bonds in both hair specimens were cleaved to eliminate the effect of the matrix using an established protocol [31]. Approximately 0.5 g of each hair was first briefly rinsed with acetone to remove surface lipids [32]. The sample was further immersed in 0.1 M 2-mercaptoethanol in 20% 1-propanol solution for 2 days. This process is necessary to remove the disulfide bonds in the matrix. The sample was then moved to 0.1 M methyl iodide in 0.2 M boric acid solution for a day after rinsing with a 50% 1-propanol in between steps. The methyl iodide helps to prevent future cross-linking in the matrix after the reduction [33]. Both samples were kept under room condition for 24 h to remove the surface moisture. This process is illustrated in Fig. 2.

2.5. Characterization

Cuticle morphologies and cross-sectional surfaces in both samples before and after treatment were observed in a FEI SFEG ultrahigh-resolution scanning electron microscope (SEM) (FEI, Hillsboro, OR). The specimens were sputtered with iridium before observation. Simultaneous thermogravimetric analysis (TGA) and differential scanning calorimetry (DSC) analysis was conducted with a TA Instruments Q600 apparatus at a constant heating rate of 20 °C min^{-1} up to 500 °C in a nitrogen atmosphere with a purge rate of 10 ml min^{-1}. A Nicolet Magna-IR 550 instrument was applied for the Fourier transform infrared spectroscopy (FTIR) analysis on both hair samples. A single-crystal diffractometer (Bruker) is applied to obtain the XRD diffraction patterns of the alpha-keratin fibers. The longitudinal axes are placed perpendicular to the X-ray beam and the diffraction patterns are therefore collected.

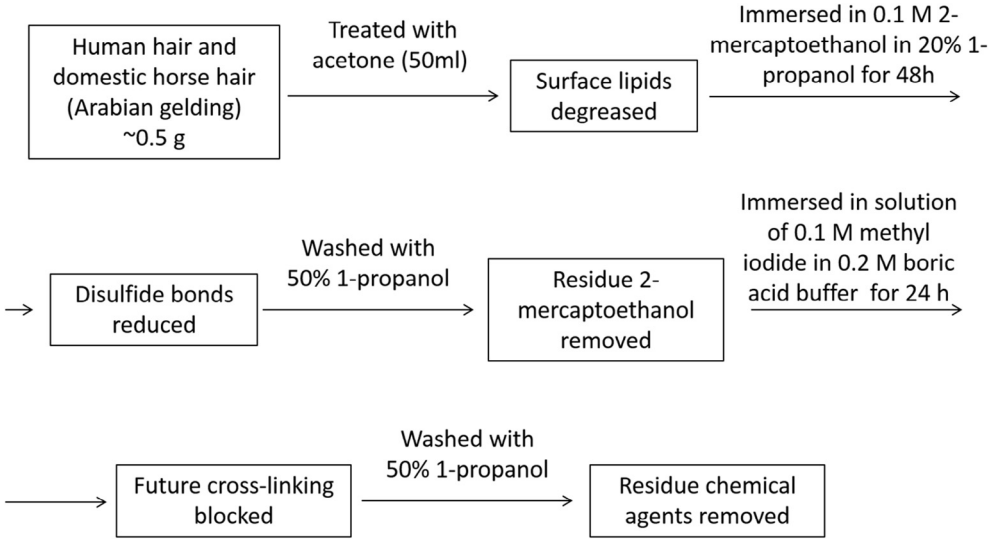

Fig. 2. Treatment process of hair specimens.

2.6. Calculation of Weibull distribution

Weibull distribution applies to the distribution of failure stresses in materials where there is a considerable variation. It is based on the precept that the material volume, V, can be divided in a number n of elemental volumes V_0, and that each one has a characteristic failure probability distribution. Probabilities of survival of an elemental volume V_0, $P(V_0)$, are calculated using the Weibull expression:

$$P(V_0) = \exp\left[-\left(\frac{\sigma - \sigma_u}{\sigma_0}\right)^m\right] \quad (1)$$

where m is the Weibull modulus, σ_u is the stress below which no failure occurs, and σ_0 is a characteristic stress at which $P(V_0) = 1/e$.

The total probability of survival of a volume V is:

$$P(V) = P(V_0)^n. \quad (2)$$

3. Results and discussion

3.1. Dynamic mechanical properties

Fig. 3 shows the storage moduli and tangent delta (equal to the ratio of loss and storage moduli) of horse and human hair at increasing frequencies and temperatures. The tangent delta parameter represents the viscoelasticity of these α-keratin fibers. As the frequency increases from 0.1 Hz to 0.42 Hz (Fig. 3a), the storage modulus of horse hair (Fig. 3b) increases from 2.86 GPa to 3.02 GPa while that of human hair (Fig. 3c) increases from 2.28 GPa to 2.51 GPa as tangent delta decreases in both hair specimens. As the frequency further increases to 2.4 Hz, the modulus only shows a gradual increase to 3.20 GPa (horse hair) and 2.73 GPa (human hair) as tangent delta decreases to 0.07 (horse hair) and 0.12 (human hair).

Both hair specimens were then tested at a fixed frequency of 0.75 Hz as the temperature was increased from 30 °C to 110 °C; the result is plotted in Fig. 3b and 3c. The storage modulus curves exhibit a two-step decrease for both hairs with a distinct change in slope: as the temperature of the chamber increases from 30 °C to ~50–60 °C, it shows a decrease from 3.2 GPa to 2.2 GPa for horse hair and from 2.4 GPa to 1.8 GPa for human hair. As the temperature further increases to 110 °C, the storage modulus eventually reaches ~1.2 GPa for both hair specimens. However, the tangent delta curve exhibits a peak at ~55 °C in both curves. The loss modulus vs. temperature curves provided in supplementary materials Fig. S1 show the peaks for both human and horse hair at the temperature of 55 °C, which correlates to the glass transition temperature of α-keratin fibers under such condition. Thus, both Fig. 3b, c and S1a, are in agreement and confirm such structural change. Therefore, the glass transition temperature of α-keratin fibers under such condition is determined to be around 55 °C. The tangent delta value further increases as the temperature increases beyond 60 °C. The structural change temperature is marked by an arrow in Fig. 3b.

The above results show that as the frequency increases, the α-keratin fibers exhibit an increase in the storage modulus and a decrease in the loss modulus, which results in an overall decrease of tangent delta. It also indicates that at higher frequencies, the α-keratin fibers behave more elastically as the degree of viscosity decreases. A similar behavior of human hair from our previous study on the strain-rate sensitivity [13] indicates that as the strain rate increases, the work of fracture increases and therefore human hair becomes tougher. This can be understood in terms of the chemical links within the hair fibers. The amorphous matrix is thought to be viscoelastic and the crystalline α-keratin is relatively strain-rate insensitive. Therefore, the crosslinks in the matrix (probably the disulfide bonds) possibly contribute to the above change in the storage modulus. Therefore, the viscoelasticity of α-keratin fibers is shown by the dynamic mechanical analysis. This will be discussed further in Section 3.2.

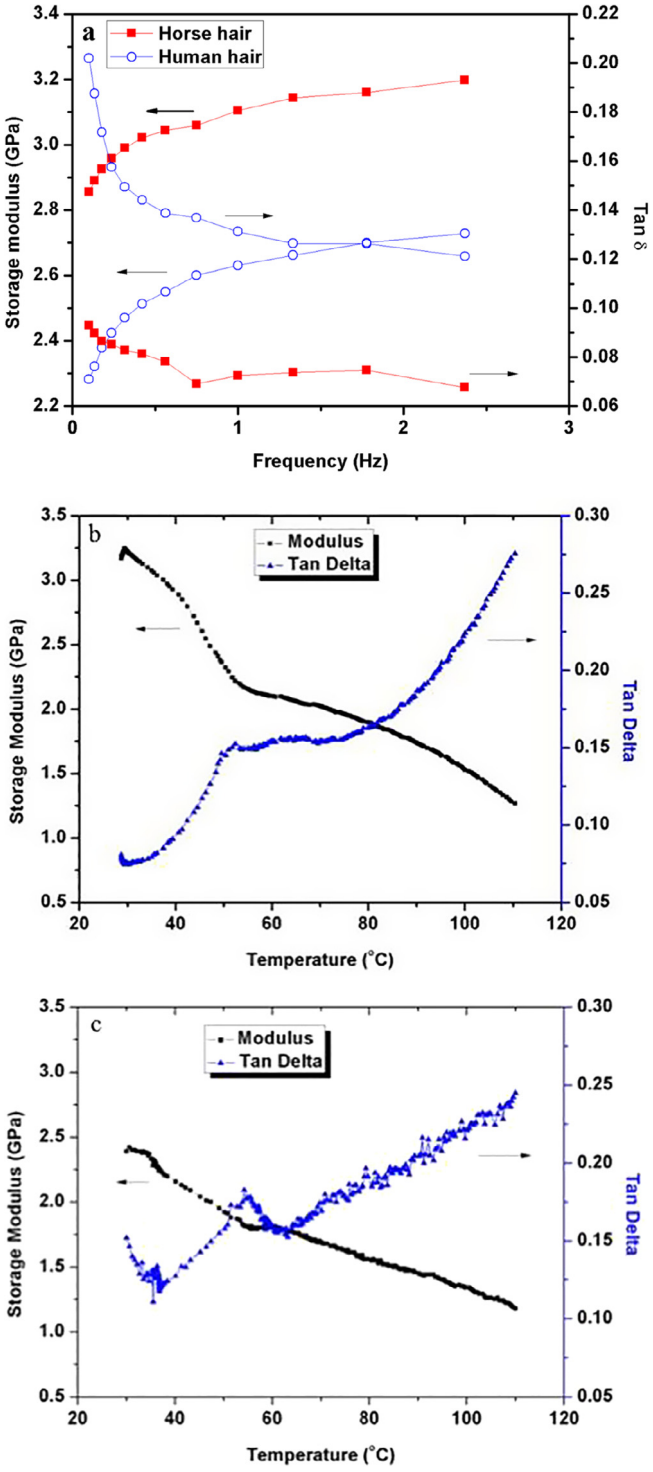

Fig. 3. (a) Horse and human hair storage modulus and tangent delta ($= \frac{loss\ modulus}{storage\ modulus}$) as a function of frequency (the storage modulus increases with frequency by virtue of the reduced time for viscous effects); (b) horse hair storage moduli and tangent delta as a function of temperature at 0.75 Hz; (c) human hair under the same conditions as (b).

3.2. Stress relaxation

Fig. 4 shows the stress relaxation curves of both horse and human hair specimens at strains of 0.02 and 0.25. These two strains were chosen to reflect different stages in the deformation: the elastic and transformation regions. As the specimens are stretched at a strain rate of $10^{-3}\,s^{-1}$ and held at different strains, the relaxation behavior shows both viscoelasticity and nonlinearity. For the specimen held at 0.02 strain, the stress reaches to 50 MPa for horse hair and 92 MPa for human hair at the beginning of the relaxation. As the relaxation starts, the stress in both hair specimens first rapidly decreases and then gradually flattens for times above 500s. However, the specimens held at 0.25 strain show a different relaxation behavior. During the initial relaxation period (~50s), the stress shows a similar decreasing rate as the specimens held at 0.02 strain; as time further increases, the stress reaches a plateau much earlier than the specimens held at 0.02. This can also be seen from the inserted figure which shows the normalized stress as a function of time. For the specimens held at 0.02 strain, the stresses keep decreasing and slowly reach 0.55 (horse hair) and 0.57 (human hair) of the initial stress (start of relaxation). For the specimens held at 0.25 strain, the stresses decrease in the beginning and rapidly reach 0.70 (horse hair) and 0.75 (human hair) of the initial stress (~200s compared to ~500s in the specimens held at 0.02). Therefore, the results show that as the α-keratin fibers are stretched to elastic and transformation regions, they exhibit different stress relaxation behaviors. This is thought to be related to keratin phase (α or β keratin) within the hair fibers during tensile tests.

The stress relaxation behavior of α-keratin hair in the elastic and transformation regions also reveals significant viscoelasticity. As hair is stretched to a strain of 0.02, only rearrangements of the bond angles within the fibers are thought to take place and contribute to the increase of strain. Our previous study [13] also confirmed that as the hair is stretched within the elastic region (0 ~ 0.02–0.05 strain), the elongation is reversible since there is no phase transformation from α-keratin to β-keratin or permanent sliding between fibers.

The viscoelasticity of α-keratin fiber can be represented by a simplified version of Maxwell-Wiechert model [34]. The relationship between relaxation modulus and time is as follows:

$$E_{relaxation}(t) = E_0 + E_1 e^{-t/\tau_1} + E_2 e^{-t/\tau_2} \quad (3)$$

where E_0 is an elastic modulus (not time-dependent), E_1 and E_2 are elastic moduli within two Maxwell elements, τ_1 and τ_2 are two relaxation constants, defined by the ratio of viscosity η and elastic modulus E in each Maxwell element, as shown in the insert of Fig. 5. This can be explained with the crystalline and elastic components in α-keratin fibers. The two-stage relaxation of stress observed above is illustrated by the two different relaxation constants (τ_1 and τ_2). The smaller constant, τ_1, contributes to the rapid decrease while the larger constant, τ_2, contributes to the gradual decrease.

According to Emile et al. [23], this two-step relaxation behavior is related to the hierarchical structure of α-keratin fibers. The fibers are mainly composed of uniaxial cortical cells, which are embedded in an amorphous matrix. Those cortical cells are further composed of macrofibrils, which are also made of intermediate filaments and an amorphous matrix. Therefore, the α-keratin fibers are made from amorphous, viscous high-sulfide matrix and crystalline, strain-rate insensitive fibrils. As previously observed [13] and shown in schematic fashion in Fig. 1, intermediate filaments with a diameter of 7 nm and macrofibrils with a diameter of 100–400 nm are the major components at the nanometer and submicrometer scale while at the micrometer scale, cortical cells of 1–6 μm are the major component. As the stress relaxation begins, the larger-scale structure (such as cortical cells) would contribute to the smaller relaxation constant in Eq. (1), therefore resulting in the rapid decrease observed. The smaller-scale structure (such as the intermediate filaments) further contributes to the larger relaxation constant. The parallel configuration between cortical cells and matrix resembles the above Maxwell-Wiechert model and this overall structure contributes to the viscoelasticity of α-keratin fibers.

Based on the experimental data from Fig. 4, the fitted relaxation modulus as a function of time is plotted and shown in Fig. 5; the equations for both horse and human hair are:

$$E_{relaxation}(t)(GPa) = 1.23 + 0.46e^{-t/14} + 0.72e^{-t/359}\ (Horse\ hair) \quad (4)$$

$$E_{relaxation}(t)(GPa) = 2.65 + 0.71e^{-t/11} + 1.26e^{-t/207}\ (Human\ hair) \quad (5)$$

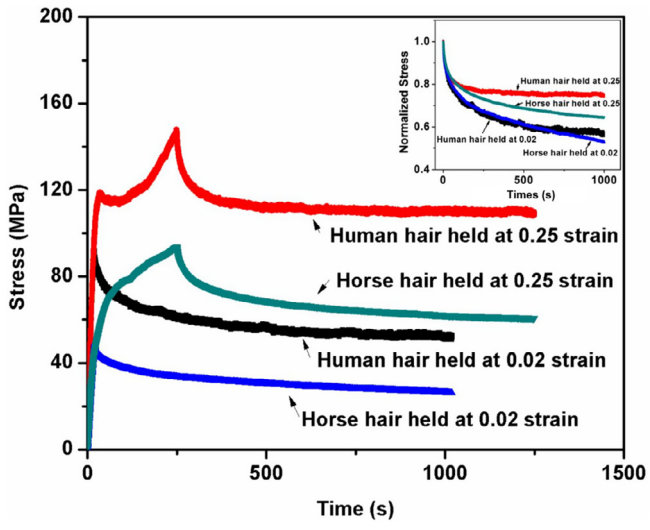

Fig. 4. Stress relaxation curves of horse and human hair specimens held at 0.02 and 0.25 strain, respectively (inserted figure shows the normalized stress as a function of time). The normalized stress represents the instantaneous stress divided by the stress at the beginning of relaxation.

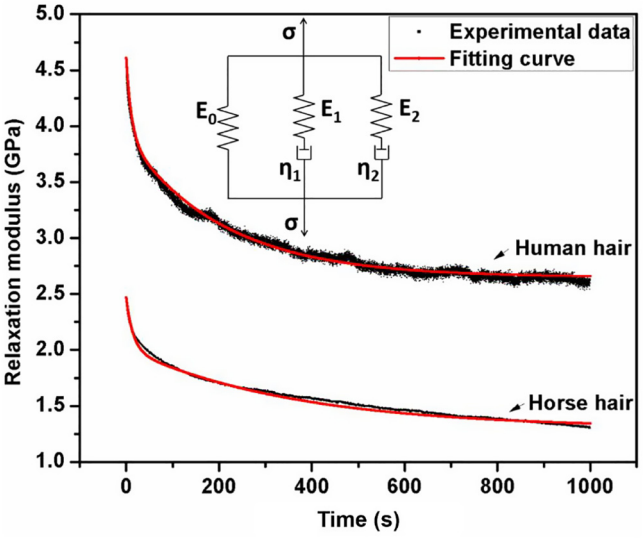

Fig. 5. Relaxation modulus curves of horse hair and human hair specimens held at a strain of 0.02 as a function of time (inserted figure shows the Maxwell-Wiechert model applied) (note that the dots represent experimental data and the solid curve represents the fitting curve).

where the time-independent elastic modulus E_0 is 1.23 GPa for horse hair and 2.65 GPa for human hair, the two elastic moduli in the Maxwell elements, E_1 and E_2 are respectively 0.46 and 0.72 GPa for horse hair and 0.71 and 1.26 GPa for human hair, the two relaxation constants, τ_1 and τ_2 are 14 and 359 s for horse hair and 11 s and 207 s for human hair. As time increases, the contribution of viscous components diminishes. Therefore, the elastic component dominates after ~500 s in the overall relaxation modulus. Meanwhile, similar to the behavior observed on spider silk [23], the larger constant is one order of magnitude higher than the smaller constant (359 s vs. 14 s and 207 s vs. 11 s), which can be explained by the dimensional difference between cortical cells and macrofibrils in the hierarchical structure of α-keratin fibers (for example in human hair, ~1–6 μm and 0.1–0.4 μm, respectively).

For the specimens strained to 0.25 and held at this strain (Fig. 4), uncoiling of the α-helices [19,24] and a possible phase transformation from α-helices to β-sheets is thought to take place during deformation. Therefore, it is possible that at the beginning of relaxation, a mix of α-keratin and β-keratin coexist in the hair specimens. As observed in our previous study [13], the deformation within this region is partially reversible. Therefore, not only do the various components (α-keratin, β-keratin, and matrix) contribute to the stress relaxation, but also the partial reversibility contributes to the decrease of stress. As mentioned earlier, the stress decreases to ~70 MPa for horse hair and ~110 MPa for human hair after ~250 s, which is close to the yield stress (~70 and ~110 MPa, respectively) (defined as the stress at a 0.02 strain offset), indicating a possible residual stress due to phase transformation from α- to β-keratin. This results in a final normalized stress of ~0.7, which is higher than the relaxation experiments at 0.02 strain (as indicated in the inserted figure in Fig. 4).

3.3. Creep

The mechanical behavior of α-keratin fibers at constant stress (Fig. 6) is analyzed for both hair specimens. The hair specimens were stretched at a strain rate of 10^{-3} s^{-1} until the stress reached 90 MPa (horse hair) and 100 MPa (human hair). These stresses were applied to ensure that the strain (~0.02) was within the elastic region at the onset of creep.

For the horse hair specimen, as the stress reaches 90 MPa, the strain first shows a linear increase to ~0.15, followed by a slower increase until rupture at the strain of 0.47. However, as the specimen enters the transformation region, several jumps of strain can be noticed from the curve (marked with dashed ellipses). For the human hair specimen, following the start of creep when the stress reaches to a set value, the curve shows a linear increase of strain up to ~0.17 (stage I as indicated), followed by a non-linear increase (stage II). As the strain increases to ~0.24, a different behavior (stage III) can be seen from the curve. During this stage, the strain does not show gradual increase as stage II. Instead, it shows a plateau followed by sudden jumps, as indicated by the dashed ellipses in Fig. 6. However, as each jump happens, the strain exhibits a partial decrease from the highest point and is further maintained at such strain. The strain increases after several cycles of such repetitive behavior and the human hair specimen finally broke at ~0.47 after ~7.5 h.

The creep test on α-keratin fibers also helps to understand the viscoelasticity and uncoiling (and possibly phase transformation) of α-helices. As the hair specimen is deformed and the stress increases to the set value, the α-keratin fiber experiences an elastic deformation up to ~0.02 strain. The strain further linearly increases to ~0.17 as the stress is maintained, which is followed by a parabolic increase to ~0.24. It is thought that during these periods, bond angle rearrangements mainly contribute to the

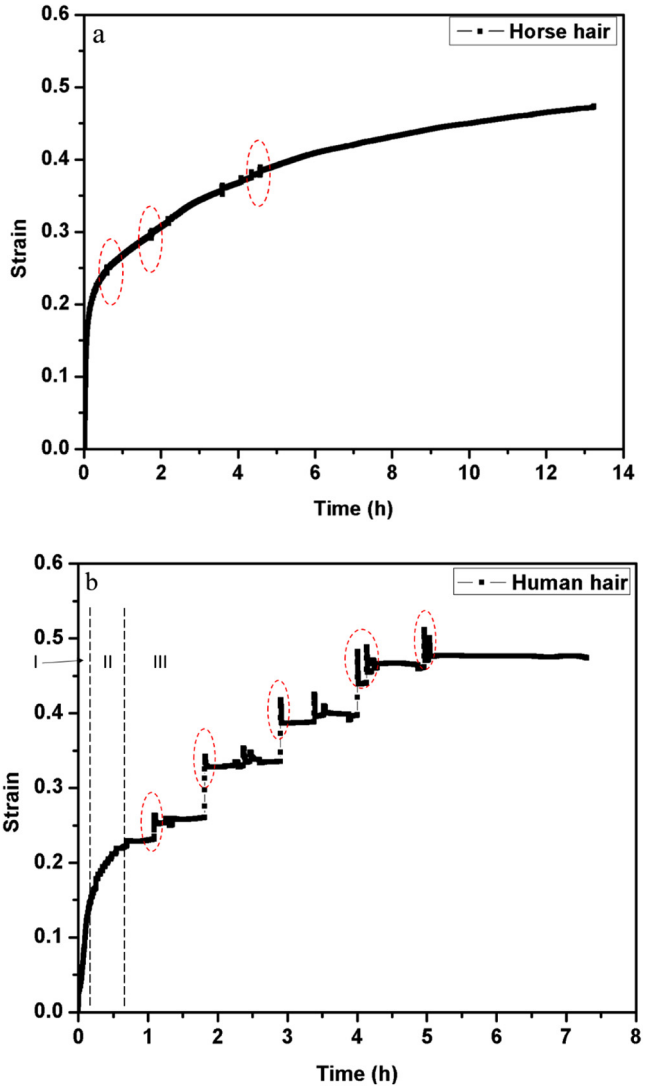

Fig. 6. Creep curve of (a) horse hair and (b) human hair under a constant stress of 100 MPa (the hair specimen was first stretched at the strain rate of 10^{-3} s^{-1} until the stress reached to 100 MPa) (note that sudden strain bursts marked by dashed ellipses). The jumps in strain occur in the 0.2–0.45 range and are attributed to unfolding of α-keratin or transformation to β-keratin.

increase of strain. However, for the human hair specimens, stage III is composed of plateaus followed by sudden increases in strain (marked by dashed ellipses in Fig. 6a and b). Such sudden 'bursts' can be explained by the uncoiling of the α-helices, which open periodically as illustrated by the model developed by Chapman [2]. The complete transformation from α-helices to β-sheets in theory results in a strain of 1.31 [13]. However, it is also observed that following each jump, there is a partial drop in strain (as shown in red ellipses), which is explained by the structure change from completely straightened to the final configuration. As shown in Fig. 7, when the α-helical structure is fully extended to the complete straightened state, the nominal strain of one such turn is higher than 1.31 because as follows

$$\frac{1.39\text{nm} - 0.52\text{nm}}{0.52\text{nm}} = 1.78\% \tag{6}$$

However, a theoretical full transformation from α-helix to β-sheet results in a strain of 1.31 [13], which gives a decrease of 0.47 in strain from the complete straightening state to β-sheet structure. Such decrease from the intermediate state is helpful in

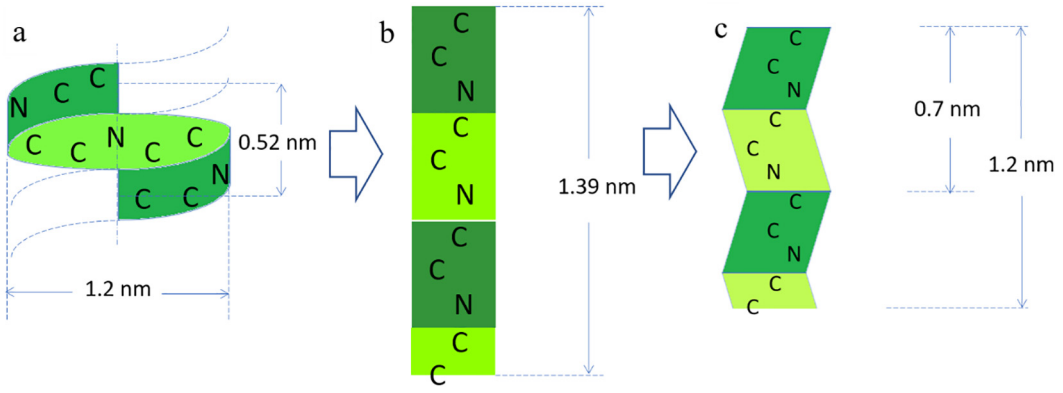

Fig. 7. Schematic representation of structure transformation from (a) α-keratin to (b) complete straightening state and to (c) β-keratin (reproduced based on [13]).

understanding the partial drop after each jump of strain. During stage III (Fig. 6b), the strain increases in such stepped manner until the human hair specimen reaches to the final breakage at 0.47, which agrees with the average breaking strains (~0.45) shown at various strain rates [13].

3.4. Tensile properties and strain-rate sensitivities

The tensile response of horse hair is studied and compared to the human hair from our previous study [13]; the results are shown in Fig. 8. Unlike human hair, horse hair does not show much increase in stress during the post-transformation region (beyond ~0.25 strain). As the strain rate increases, the Young's modulus in the Hookean region mainly remains the same, while the yield stress exhibits little increase with an increasing strain rate (Fig. 8a). Human hair has a yield stress (defined as the stress at 2% offset) changing from 43 MPa (at 10^{-4} s^{-1}) to 126 MPa (at 10^{0} s^{-1}), resulting in a strain-rate sensitivity of 0.11 [13]. On the other hand, the yield stress of horse hair is approximately 91 MPa and 135 MPa at strain rates of 10^{-4} s^{-1} and 10^{0} s^{-1}, respec-

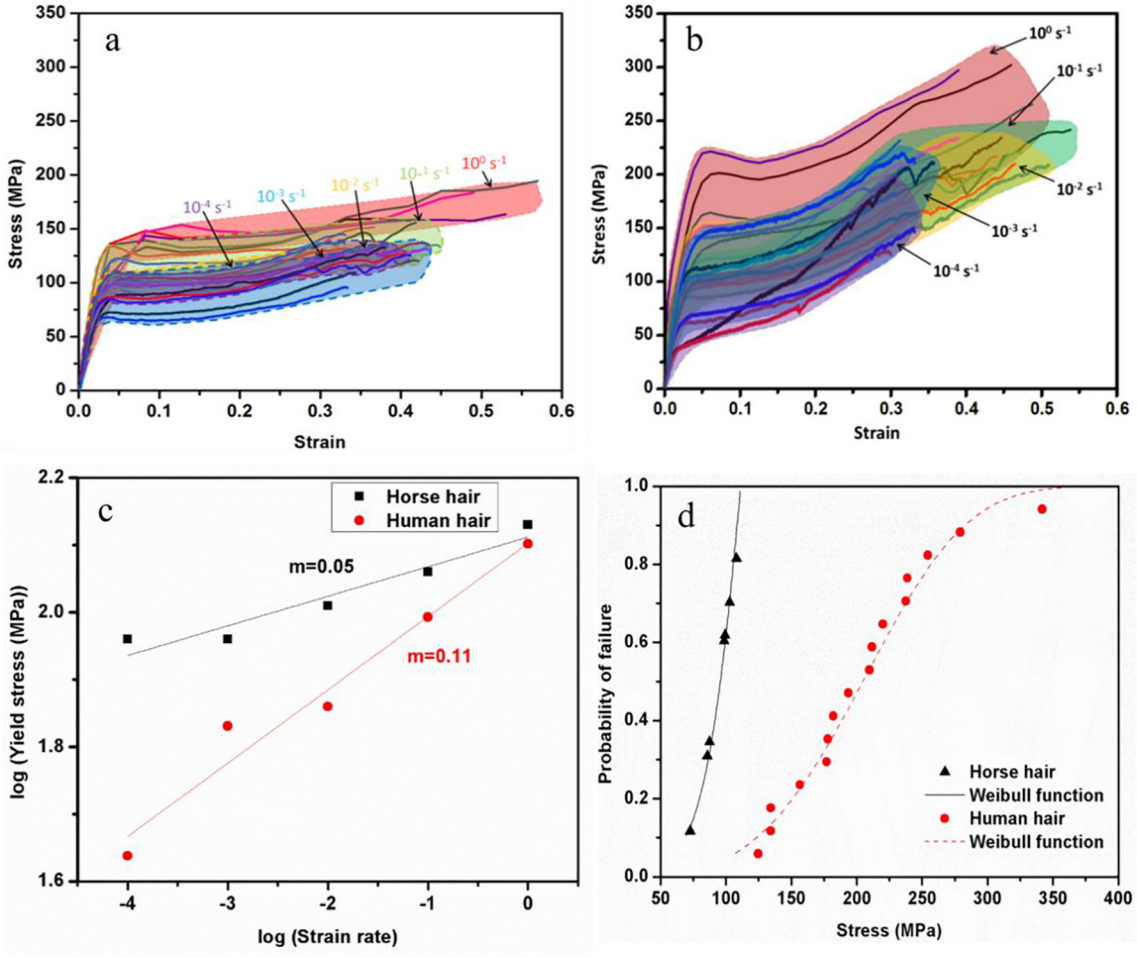

Fig. 8. Band plots of tensile results of (a) horse hair, (b) human hair adapted from [13], (c) strain rate sensitivities and (d) Weibull analysis of both hair (note lower strengths of horse hair and strain-rate sensitivity).

tively. The increase in the work of fracture with strain rate observed for both human and horse hair is a direct result of the decrease in the viscous component which results from sliding between fibers and cells (at different hierarchical levels). Decreased sliding will result in higher strength and also, as observed in Fig. 8a and b, increased strain-to-failure.

Fig. 8c shows that horse hair exhibits a strain-rate sensitivity of 0.05, which is much smaller than that of human hair. Since both horse and human hairs are similar α-keratin fibers, it is worth understanding the reasons of such different strain-rate sensitivities.

Fig. 8d shows the Weibull distributions of the breaking stresses of horse and human hair at the strain rate of 10^{-2} s^{-1}. At the 50% probability of failure, human hair shows a breaking stress of 205 MPa, which is much higher than the stress of horse hair, 95 MPa. This can also be seen from the band plots (Fig. 8b); human hair has a higher breaking stress. On the other hand, the Weibull modulus (m) of human hair is 3.72, which is smaller than that of horse hair, 6.55. As the Weibull modulus increases, the data exhibit a much smaller variability and the performance is more stable [35]. These results show that human hair has a less stable response, but generally is much stronger than horse hair. As horse hair has a larger cross-sectional area, a much larger force is required to bend the fibers; this represents structural stiffness. That helps to explain why horse hair is applied in various applications such as brushes, but not human hair.

The fracture strains of hair (both human and horse) are in the range 0.4–0.6, which is exceptionally considering their strength. These large values are due to the plateau region of the stress-strain curves, which is followed by more intense hardening and subsequent fracture. The uncoiling and/or transformation to beta sheets is an additional mechanism of inelastic deformation. Although there is some damage associated with this stage, it is not as extensive as the other damage processes. We have shown previously (Yu et al. [13], Fig. 8) that some damage occurs when specimens are loaded up to the plateau region and subsequently unloaded. However, there is definitely an increase in the fracture strain due to the plateau mechanisms.

3.5. Morphology and crystal structure

Since the cuticle morphology and conditions are highly related to the living environment [36], horse and human hair exhibit significantly different surface structures. Fig. S2 (Supplementary Information) compares the cuticle edges in both specimens. Horse hair (Fig. S2a) shows much more damaged cuticle edges with cracks in some cuticle sheets (shown by arrows). This is understandable since horse hair is rarely moistened and taken care of. The tail whips around to swat away flies. On the other hand, human hair (Fig. S2b) shows a very smooth surface with only occasional lifting in the natural condition. However, since cuticles have been shown not to largely affect the tensile properties even in broken or damaged condition [37], this difference in surface morphology cannot account for the differences in the tensile properties between these two hair fibers.

Fig. 9 shows the surface morphology of a cortical cell in human hair after tension. The surface exhibits a suture-like structure, which greatly increases the surface area and contact area of cortical cells and therefore increases the adhesion between adjacent cells. Moreover, the suture structure, with a width of several hundred nanometers, creates an interlocking effect, as previously shown in pangolin scales [38] and generalized by Naleway et al. [39]. As the hair is stretched under tension, this structure mechanically decreases the sliding between cortical cells.

Fig. 10 shows the cross-sectional area of a human hair fiber after failure in tension. Four layers of cuticle sheets can be identified in Fig.10a. These cuticle sheets overlap, as indicated by the arrows. An enlarged SEM micrograph (Fig.10b) shows that the cuticle structure exhibits a strong adhesion between the sheets, which leaves no spacing even after the hair is fractured in tension. The flexure modulus has been found to decrease as the cuticles are damaged, but the tensile modulus remains unchanged [40]. The principal function of the cuticles is to ensure the integrity of the hair. If it is removed, the fibers tend to split apart. In flexure, the fibers subjected can undergo buckling and separate, in the absence of the cuticle. This can result from excessive brushing and leads to 'split ends'. Fig.10c and d show the effect of the cuticle.

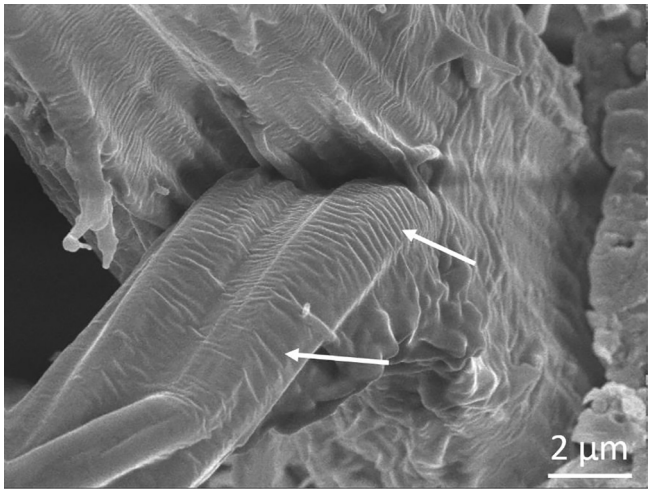

Fig. 9. Scanning electron micrograph (SEM) of cortical cell surface in a tensioned untreated human hair fiber (arrows indicate the suture-like morphology).

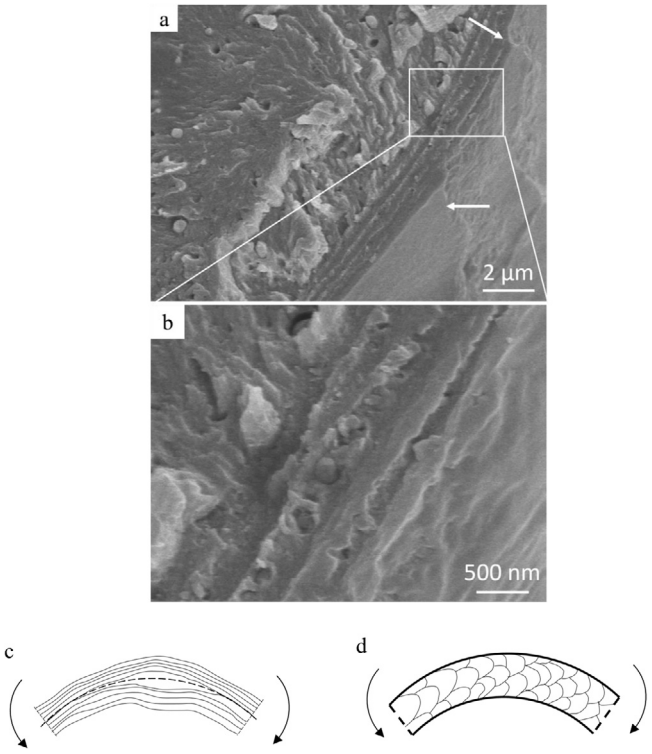

Fig. 10. Scanning electron micrographs (SEM) of (a, b) cortical cell surface in a tensioned untreated human hair fiber (note the layered structure of cuticles) (arrows indicate the edge of one cuticle sheet); (c) bending of cortex in the absence of cuticle and buckling in compression side; (d) bending with cuticles. They act as confinement structures preventing splitting.

Wide-angle X-ray diffraction (XRD) patterns of horse and human hair are shown in Fig. S3. Both hairs exhibit a similar pattern. First, a meridional spacing reflection at 0.52 nm indicates the α-helix pitch projection along the coil axis [8]. However, this arc is further superimposed to a broad ring at ~0.5 nm. According to Busson et al. [41], this is due to a less ordered structure from the coiled coils. Second, a broad equatorial reflection at ~0.96 nm indicates the distance between various α-helical chains. Since α-keratin exhibits a much different diffraction pattern than β-keratin [24], these results show that horse and human hair are both composed of α-keratin and a similar crystal structure exists in these hair specimens.

3.6. Thermal and FTIR analysis

Thermogravimetric analysis (TGA) and differential scanning calorimetry (DSC) were further conducted to understand the similarities and differences in the two hair fibers. The results of these characterizations are shown in Fig. 11. Fig. 11a shows the TGA data of horse and human hair. The initial weights of these samples are 10.99 mg and 13.79 mg, respectively. Both hairs exhibit a similar trend in weight loss: an initial slower loss from 20 °C to 220 °C followed by another significant decrease in weight from 220 °C to 500 °C. It has been shown that the first decrease is due to the evaporation and loss of the bound water in the fibers [42]. Both samples lost ~15% of weight as water evaporated. The further weight decrease in both curves is related to the denaturation of the keratin and degradation of the organic components, which generates a rapid material loss from 220 °C to ~320 °C and a slower decrease further up to ~400 °C. The TGA two-stage configuration is similar to the one observed for wool by Idris et al. [43]. After 400 °C, there was some residue from the fibers; the resulting weight left in horse and human hair is 23% and 26%, respectively. These results show that there is little difference in the organic components between the two hair fibers.

DSC data examines the stability of specimens within a specific temperature range. Fig.11b shows the comparison between the two fibers. The first endotherm in the curve of human hair exhibits a peak from ~50 to ~90 °C, a result from water evaporation [44,45]. On the other hand, horse hair has a much wider peak at a higher temperature range (~70 – 120 °C). The higher temperature peaks in both curves show the denaturation of the keratinous structures. Similar phenomena were also observed by Balaji et al. [46] for keratin-collagen scaffold, which also confirms our results. Human hair has been reported to exhibit such peak at ~220 °C, while horse hair shows a much wider peak ranging from ~220 to ~270 °C. These results indicate that although horse and human hair have similar compositions, they exhibit some structural differences within or between the components. The wide peak shown in horse hair fibers indicate a longer range of heat intake than human hair, which may be related to the larger content of crystal components (intermediate filaments) in horse hair fibers, as they may require more heat to degrade.

To understand the reasons for the above differences in the mechanical properties, FTIR analysis was conducted to investigate

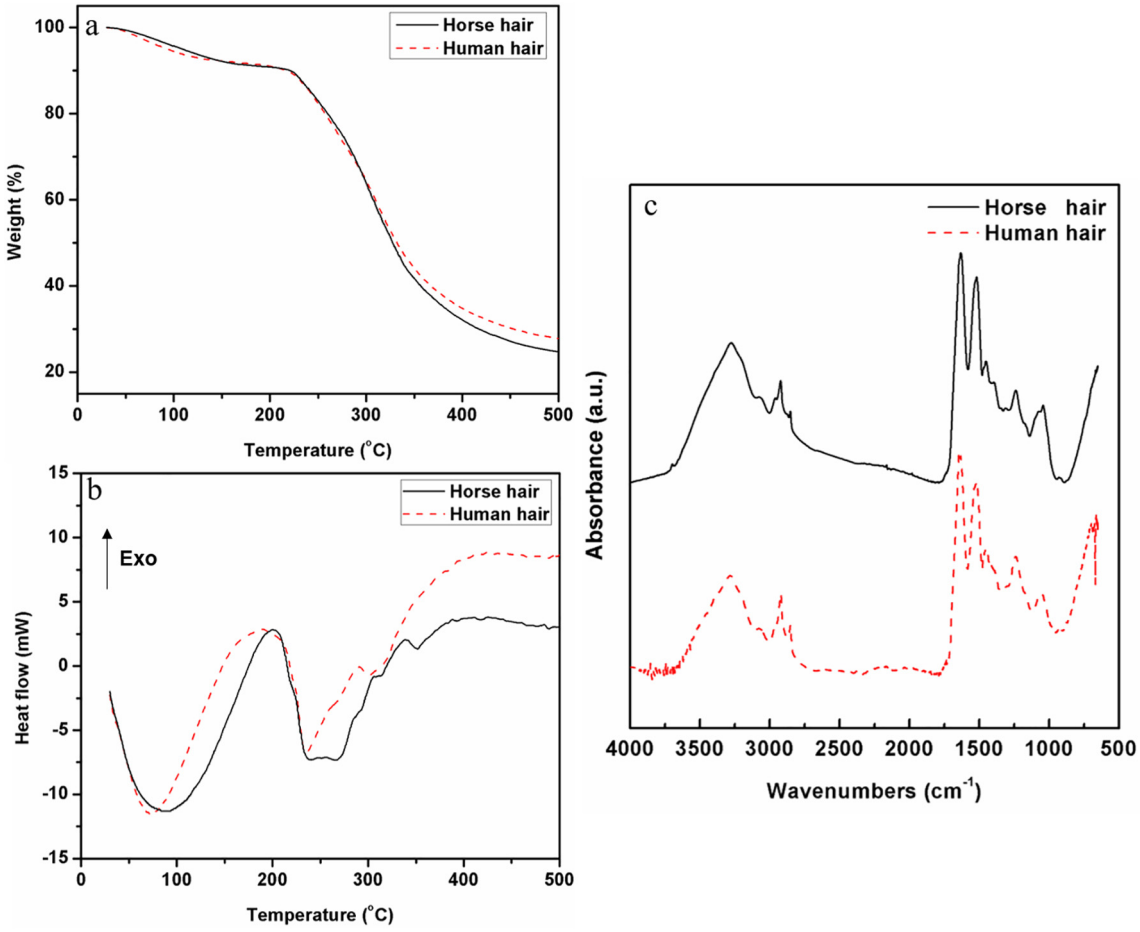

Fig. 11. Comparison of TGA, DSC, and FTIR scans for of horse and human hair showing almost identical responses. (a) TGA showing two regimes: a slightly descending plateau with decrease in weight due to evaporation of water and a much decreased slope starting at 200 °C corresponding to denaturation of alpha keratin; (b) DSC with first endothermic peak (at 75–100 °C due to evaporation of water) and first exothermic peak (at ~200 °C) due to the denaturation of crystalline alpha keratin; (c) FTIR analysis showing Amide A (at ~3300 cm^{-1}), I, II, and III (between 1600 and 1250 cm^{-1}) absorption bands.

a possible variation in the composition of chemical groups (Fig. 11c). Along the whole spectrum, several groups are especially analyzed: N–H stretching at ~3,300 cm^{-1}(amide A), CH_2 stretching at 1451 cm^{-1}, amide III at 1231–1235 cm^{-1}, cystine dioxide at 1121 cm^{-1}, cystine monoxide at 1071 cm^{-1}, cysteic acid at 1042 cm^{-1}, and cysteine-S-thiosulfate at 1022 cm^{-1} [47–49]. These groups attract more interest due to their involvement in the formation of disulfide bonds. Results show that two of the most prominent differences in peak intensity are the cysteic acid and cystine monoxide. Horse hair is thought to have a large concentration of cysteic acid and cystine monoxide, resulting from a higher oxidation of the cystine disulfide cross-links. Therefore, these data show that, in general, horse and human hair are composed of the same chemical groups. However, it is possible that the differences in composition and component ratios affect the mechanical properties of α-keratin fibers.

3.7. Morphology of treated α-keratin fibers

Since the differences in the mechanical properties are not explained by the crystal structure and chemical components, both hairs were chemically treated to remove the contribution of matrix in the viscoelasticity. SEM images were taken on horse (Figs. S4a and b) and human hair (Figs. 4c and d) to understand the effect of this treatment on the inner morphology and investigate if this process changes the physical structure. Before treatment, both specimens show a continuous cortex with hollow cavities indicating the medullar structure (Figs. S4a and S4c). After the treatment, these hair specimens exhibit a similar internal morphology (Figs. S4b and S4d). Therefore, it is confirmed that the treatment does not affect the internal physical structure and the hair fibers still maintain their original morphology. It is concluded that the reduction process only affects the chemical groups and the effect on the mechanical properties is not achieved by changing the physical structure (such as dissolving the cortex).

Fig. 12 shows the cuticle lifting of a treated human hair fiber after tension. As indicated by the arrows, the cuticle edges are largely lifted after testing. As the hair fiber is stretched, the different extensibilities in the cuticle structure lead to the lifting of the cuticle edges (Fig. 12b). This phenomenon has also been observed in our previous work with untreated human hair [13].

3.8. FTIR analysis and strain-rate sensitivities of treated α-keratin fibers

Targeted FTIR analysis on the horse and human hair specimens was conducted at a few related chemical groups. Fig. 13 shows the spectra with wavenumbers ranging from 2000 cm^{-1} to 800 cm^{-1}. The peak of amide III at 1231–1235 cm^{-1} is used as reference since it is not affected during the reduction process. For horse hair (Fig. 13a), the peak of cysteic acid at 1040 cm^{-1} and cystine monoxide at 1071 cm^{-1} remained unchanged after the treatment, while the human hair (Fig. 13b) shows much increased peak intensities at these two regions (cysteic acid and cystine monoxide). As the disulfide bonds are dissected, cystine monoxide and cystine dioxide are created as an intermediate product, while cysteic acid is produced as the final product from the disulfide bonds. The reaction below shows the. S-S cleavage mechanism (reproduced based on [50]):

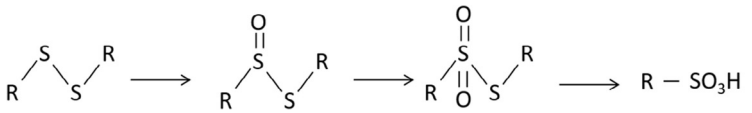

(7)

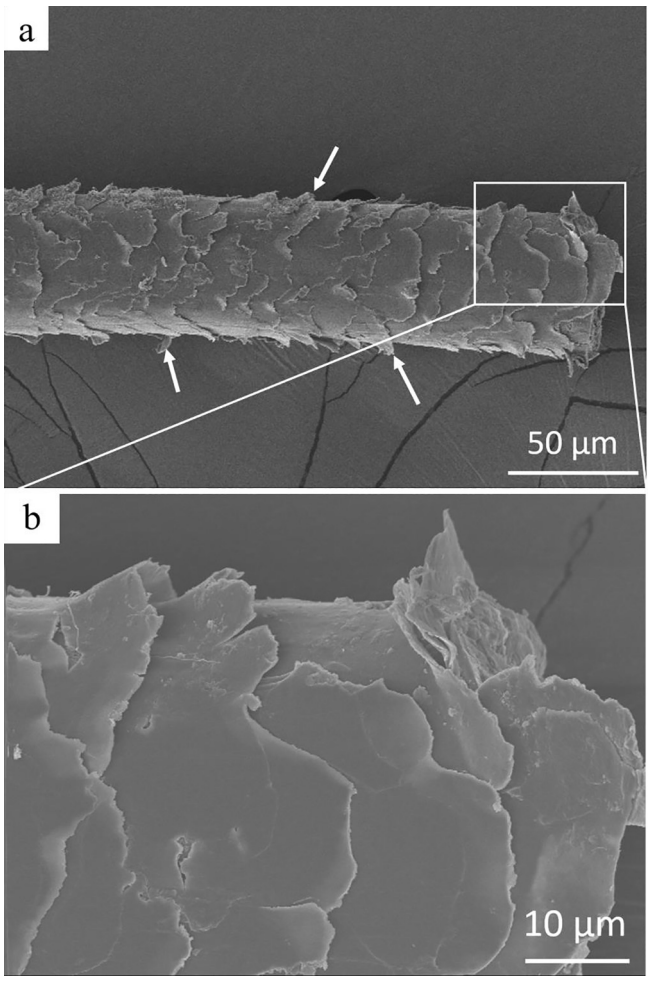

Fig. 12. Scanning electron micrographs (SEM) of (a, b) cuticle morphology of treated human hair after tension (arrows indicate the lifted cuticles).

Compared to horse hair, in which the concentrations of cysteic acid and cystine monoxide are not largely affected by the treatment, human hair exhibits a larger content increase in these two groups. Therefore, it is confirmed that among these two hair specimens, the original human hair has a larger concentration of disulfide bonds (–S–S–). Horse hair exhibits a minimal peak increase from disulfide bond cleavage, indicating that it has very low disulfide bond concentration before treatment.

The tensile strength vs logarithm of strain rate for horse and human hair are shown in Fig. 14a and b, respectively. It can be seen the m, the slope of the linear relationship, does not change significantly with chemical treatment for horse hair, whereas the human hair exhibits a substantial change. This explains the changes in strain-rate sensitivity of horse and human hair with treatment (Fig. 14b). It is also worth of noticing that, after the treatment, both horse and human hairs show a very similar sensitivity of ~0.05–0.06. As both hairs were chemically treated, the disulfide bonds were largely dissected and no longer affect the viscoelasticity of the α-keratin fibers. Therefore, the mechanical properties at this stage mainly reflect the properties of the crystalline α-helix, which

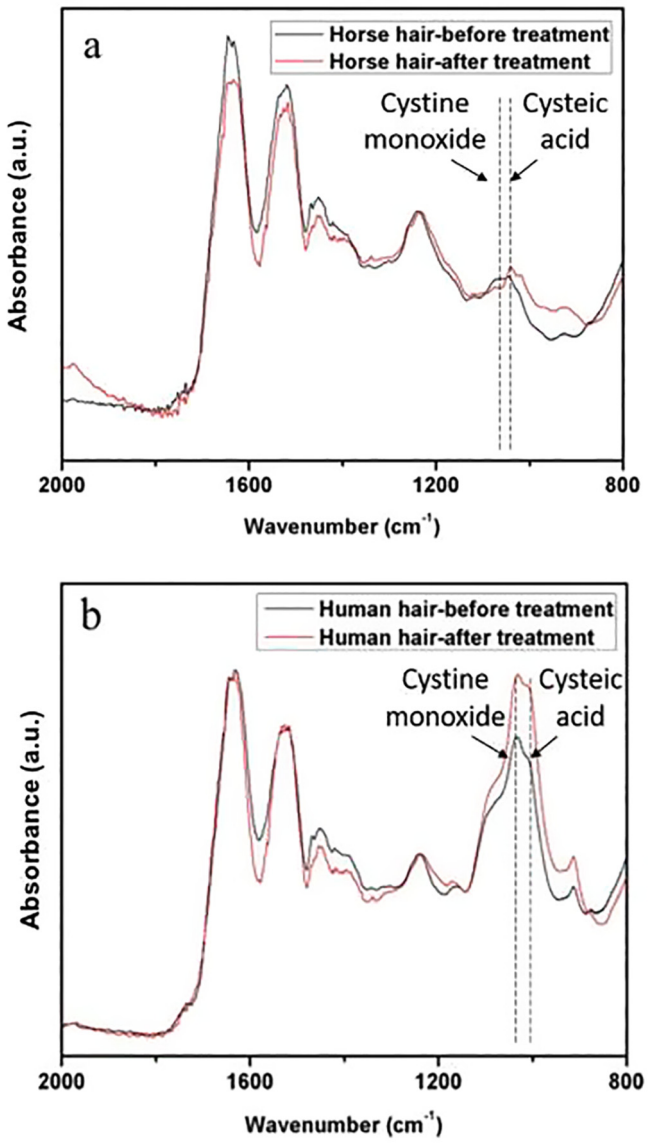

Fig. 13. FTIR analysis at the affected chemical groups of (a) horse and (b) human hair.

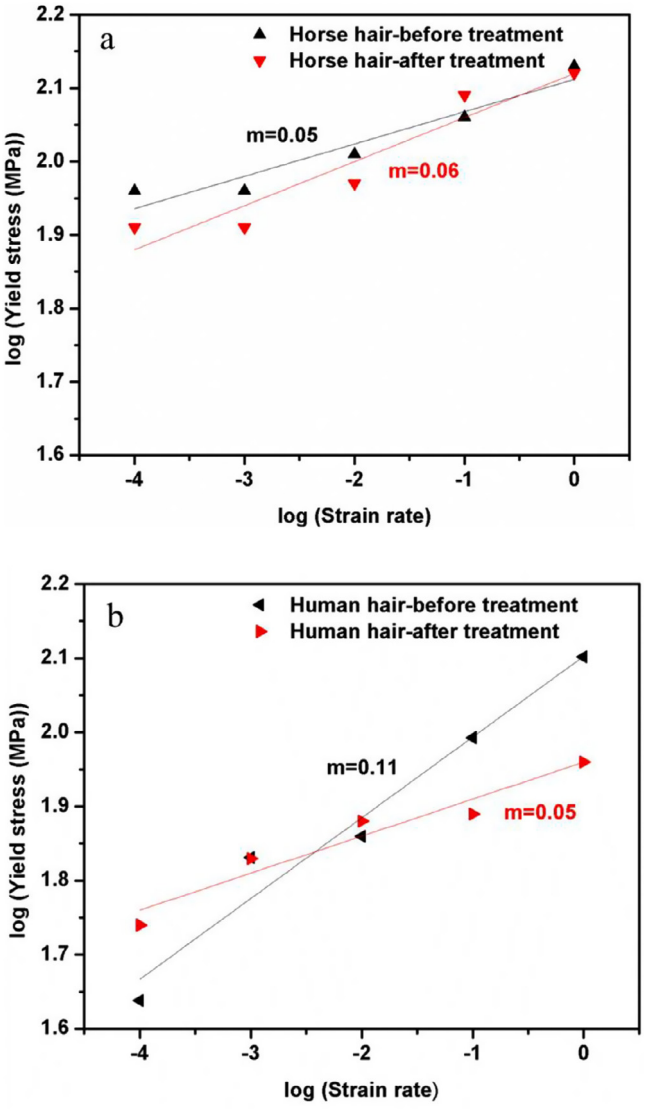

Fig. 14. Comparison of strain rate sensitivities (m) before and after treatment of (a) horse and (b) human hair, whereas m remains unchanged in horse hair, there is a large decrease in human hair.

is not so sensitive to changes in strain rate. This is thought to be helpful in explaining the similar strain-rate sensitivities of both treated hair fibers and decreased sensitivity of human hair after the treatment.

3.9. Mechanism of strain-rate sensitivity change

In order to interpret the mechanical properties of α-keratin fibers in wool and hair, different models were proposed by Feughelman [51,52]. The mechanical response of wool is reviewed by Hearle [53]. Our previous paper dealt in detail with the constitutive response of hair [13]. We focus exclusively on the effect of chemical treatment on the strain-rate sensitivity of hair here.

After the treatment, most disulfide bonds in the horse and human hairs were chemically cleaved (Fig. 15b and d). Since the horse hair has a lower disulfide bond content, the strain-rate sensitivity was not much affected (Fig. 15a). However, the human hair was largely affected by the chemical treatment, which is illustrated in Fig. 15d. As the disulfide bonds were cleaved, the intermediate filaments became more dominant in the viscoelasticity. Therefore, the human hair specimens show a decreased strain-rate sensitivity. Moreover, the treated human hair exhibits a similar sensitivity (0.05) to horse hair (~0.05), which represents the mechanical property of intermediate filaments. The treated human hair shows a higher yield stress at the strain rate of 10^{-4} s^{-1} and lower yield stress at the strain rates of 10^{-1} s^{-1} and 10^{0} s^{-1}, which indicates that for the original human hair, the yield stress is more dominated by the matrix and disulfide bonds. After the hair is treated, the disulfide bonds are dissected. The intermediate filaments become more dominant in the yield stress and mechanical property, which explains the different changes in the yield stress of human hair at lower and higher strain rates, as shown in Fig. 15b. Details of the mechanism of the viscoelasticity in both horse and human hair are summarized in Fig. 15a–d.

3.10. Hydration effects and FTIR analysis of saturated and saturated-dried human hair

Our previous study [13] shows that when the human hair specimens are tested in water, both the yield stresses at various strain rates and strain-rate sensitivity decrease compared to the air con-

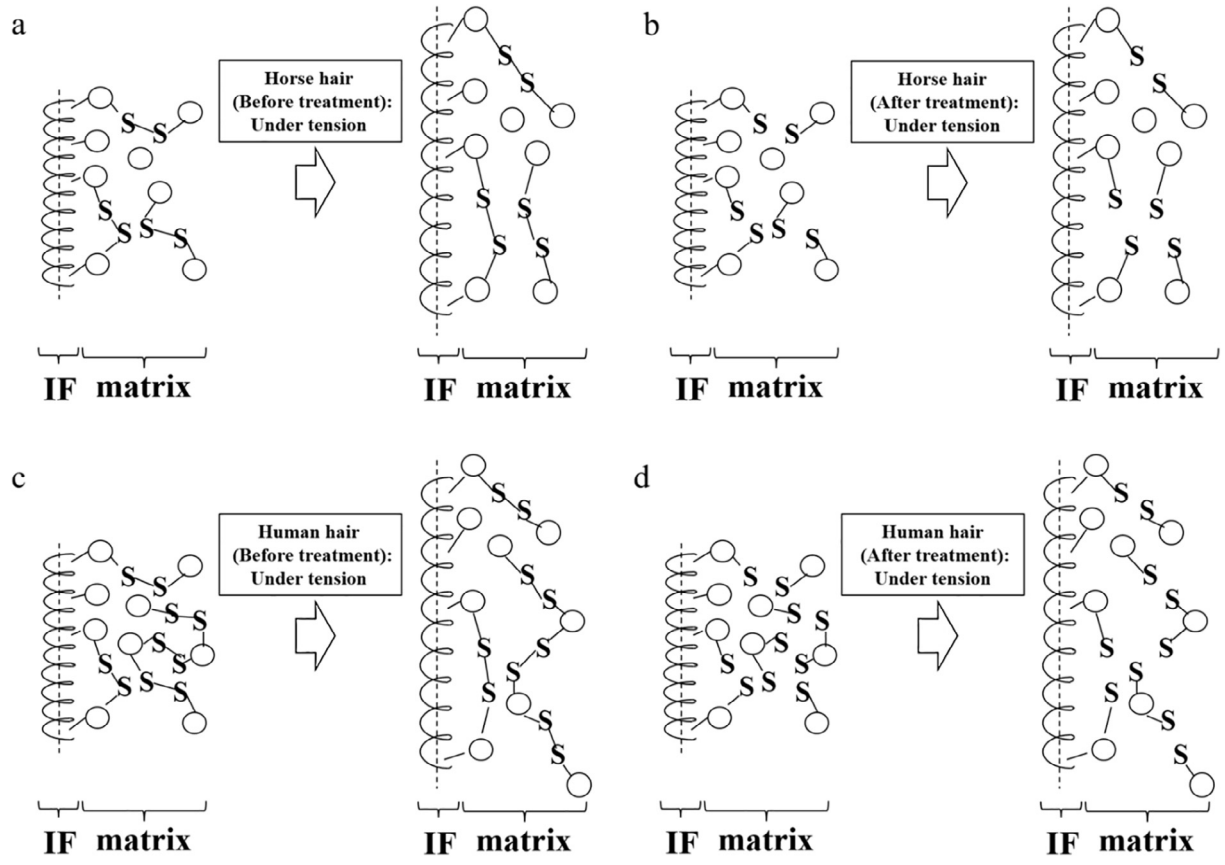

Fig. 15. Schematic drawings of the structural changes in (a, b) horse and (c, d) human hair before and after treatment. Note that the human hair has a higher concentration of the disulfide bonds; the intermediate filaments are connected to the matrix through bonds, while the 'beads' in the matrix are intermittently connected through disulfide bonds.

dition at the same temperature. The difference in the strain-rate sensitivity of the saturated human hair is further analyzed through FTIR analysis, which is also discussed by Pande et al. [54] and Joy et al. [55] and is shown in Fig. S5. As the hair is fully saturated, the peak intensities of cysteic acid and cystine monoxide increased as compared to original human hair. However, the saturated-dried hair specimen shows similar peak intensities as the original hair, which indicates that the effect of saturation is reversible after the water evaporates from the hair specimens.

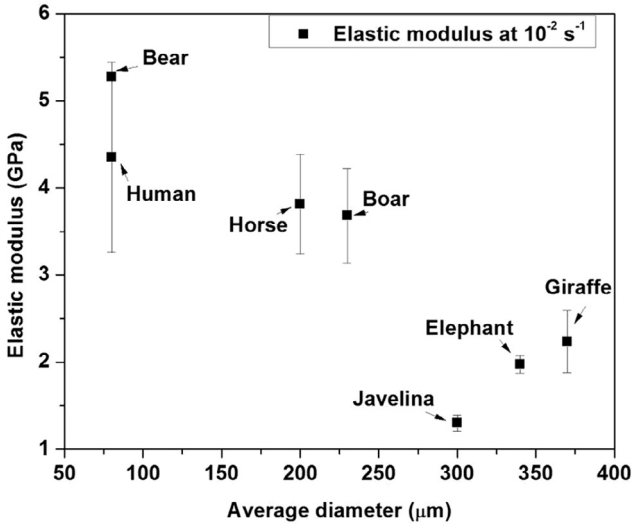

Fig. 16. Elastic modulus as a function of diameter for seven species. Note the decrease in Young's modulus with increasing diameter.

Water works as a plasticizer in hair, causing a swelling of the matrix. Feughelman [56] indicated that water affects the distance between intermediate filaments themselves and the distance between matrix and intermediate filaments. Therefore, as Fig. 15 shows, it is suggested that as the hair is fully saturated, the swelling causes an increase in the amounts of cysteic acid and cystine monoxide. It is thought to be achievable through the interaction of the disulfide bonds with the water molecules in the matrix; possibly the water molecules increase the distance of the sulfide atoms to weaken the bonds. However, as the saturated hair is further dried, the water content in the matrix is decreased and the result shows a decrease of the cysteic acid and cystine monoxide until they reach the original contents. This is helpful to understand the decreased yield strength and strain-rate sensitivity [13] since water affects the cross-link in the matrix and interaction between matrix and intermediate filaments. As the disulfide bonds are weakened, the saturated hair shows a strain-rate sensitivity of 0.06, which is comparable to that of horse hair and treated human hair.

3.11. Effect of diameter on elastic modulus

Different organisms usually have hair fibers of different diameters. In order to investigate the effect of hair diameter on the mechanical properties, wild boar, javelina, bear, Asian elephant, and giraffe are also studied. The effect of hair diameter on Young's modulus is shown in Fig. 16. The Young's modulus of the javelina falls below the others because it has inner porosity and contains

both black and white segments; failure occurs in the white regions. Šimková et al. [57] mention that darker hair is stronger because of the melanin.

There is, in agreement with the flawed results of Šimková et al. [57], a decrease in Young's modulus. This will be analyzed in a future paper in terms of Weibull statistics which has a volume dependence of strength distribution, as shown by Eq. 1.

4. Conclusions

In this present investigation, different mechanical properties and strain-rate sensitivities of two α-keratin fibers, horse and human hair, are studied. Both hair specimens are chemically treated to remove the contribution of matrix to viscoelasticity. The major findings are summarized as follows:

(i). α-keratin fibers, including both horse and human hair, behave more elastically and less viscously when tested at high frequencies. Meanwhile, as the temperature increases, α-keratin fibers exhibit a more viscous behavior, with a glass transition at ~55 °C.

(ii). As the α-keratin specimens are stretched to 0.02 strain and held at such constant strain, they show a decrease in stress with two relaxation constants. This behavior can be explained by the hierarchical structure and different levels of the filaments in the α-keratin fibers. An equation based on the Maxwell-Wiechert model with two viscous elements in parallel is used to model the stress relaxation. It agrees reasonably with the experimental data. However, as the α-keratin fibers are stretched and held at 0.25 strain, a possible phase transformation from α- to β-keratin takes place, decreasing the relaxation. The smaller time constant (11–14 s) corresponds to the viscosity of the amorphous matrix surrounding the cortical cells whereas the large time constant (207–359 s) corresponds to sliding between the intermediate filaments.

(iii). The creep behavior of α-keratin fibers is composed of three stages: a linear region, a parabolic region and a steady region. However, in the human hair specimens, the curve shows a repetitive plateau-sudden jump behavior. It is proposed that the uncoiling to the complete straightened state and possible phase transformation of the α-helical structure into β-sheets produces the effect observed in this region. The strain increases as various locations in the α-helices uncoil and transform until the hair specimen reaches breakage at ~0.47 strain.

(iv). XRD patterns, TGA, DSC and FTIR analysis on both hair specimens show that the horse and human hair are α-keratin fibers similar in terms of composition and chemical groups. However, the DSC data show that there could be possibly different bonding properties within these two hair specimens.

(v). Horse and human hairs were both treated to cleave the disulfide bonds. The strain-rate sensitivities and tensile properties were both evaluated before and after the treatment. The human hair shows a much decreased sensitivity after treatment, while the horse hair shows little difference. The FTIR data further confirms that it is due to the different disulfide bonds content, which affects the viscoelasticity in these α-keratin fibers. This difference in the disulfide bonds, resulting from the different contents in the original fibers and weathering conditions, is shown to contribute to the different strain-rate sensitivities in the α-keratin fibers.

(vi). Water affects the viscoelasticity and strain-rate sensitivity of the α-keratin fibers. In the fully saturated state in water, both yield stress and strain-rate sensitivity of human hair decrease due to the interaction between water molecules and the disulfide bonds in the matrix. However, this effect is shown to be reversible after the humidity of hair reaches an equilibrium with the room condition.

(vii). We confirm earlier results [57] that the hair diameter influences its strength and elastic modulus. Both decrease with diameter, as is inferred from evaluating hair from different species.

Acknowledgements

We thankfully acknowledge the financial support from a Multi-University Research Initiative through the Air Force Office of Scientific Research (AFOSR-FA9550-15-1-0009) and Powell Foundation through Jacobs School of Engineering at UCSD. We appreciate the help from Nicole Chan and Mike Denny for their assistance in TGA, DSC and FTIR measurements. We appreciate the help given by Nancy Guo in procuring the elephant and giraffe hair and that from Norbert and Betsy Schultz family in procuring the bear, boar, and javelina hair. We thank Haocheng Quan and Zezhou Li for their input and discussions on the stress relaxation model.

Appendix A. Supplementary data

Supplementary data associated with this article can be found, in the online version, at http://dx.doi.org/10.1016/j.actbio.2017.09.012.

References

[1] W.G. Crewther, The effects of disaggregating agents on the stress-strain relationship for wool fibers, Text. Res. J. 42 (1972) 77–85.
[2] B.M. Chapman, A mechanical model for wool and other keratin fibers, Text. Res. J. 39 (1969) 1102–1109.
[3] M. Feughelman, Mechanical Properties and Structure of Alpha-keratin Fibres: Wool, Human Hair and Related Fibres, UNSW Press, Sydney, 1997.
[4] T.A. Dankovich, Y.K. Kamath, S. Ruetsch, Tensile properties of twisted hair fibers, J. Cosmet. Sci. 55 (Suppl) (2004) S79–S90.
[5] G.V. Scott, C.R. Robbins, Stiffness of human hair fibers, J. Soc. Cosmet. Chem. 29 (1978) 469–485.
[6] I.P. Seshadri, B. Bhushan, In situ tensile deformation characterization of human hair with atomic force microscopy, Acta Mater. 56 (2008) 774–781.
[7] L.J. Szewciw, D.G. de Kerckhove, G.W. Grime, D.S. Fudge, Calcification provides mechanical reinforcement to whale baleen alpha-keratin, Proc. R. Soc. London. Ser. B, Biol. Sci. 277 (2010) 2597–2605.
[8] B. Wang, W. Yang, J. McKittrick, M.A. Meyers, Keratin: structure, mechanical properties, occurrence in biological organisms, and efforts at bioinspiration, Prog. Mater. Sci. 76 (2016) 229–318.
[9] J. McKittrick, P.-Y. Chen, S.G. Bodde, W. Yang, E.E. Novitskaya, M.A. Meyers, The structure, functions, and mechanical properties of keratin, JOM 64 (2012) 449–468.
[10] J.A. Swift, Human hair cuticle: biologically conspired to the owner's advantage, J. Cosmet. Sci. 50 (1999) 23–47.
[11] M.V.R. Velasco, T.C. De Sá Dias, A.Z. De Freitas, N.D.V. Júnior, C.A.S. De Oliveira Pinto, T.M. Kaneko, A.R. Baby, Hair fiber characteristics and methods to evaluate hair physical and mechanical properties, Brazilian, J. Pharm. Sci. 45 (2009) 153–162.
[12] D. Rivett, C. Ward, L. Belkin, J. Ramshaw, J. Wilshire, The Lennox Legacy: The History of the CSIRO Laboratory at 343 Royal Parade Parkville, Cisro Publishing, 1996.
[13] Y. Yu, W. Yang, B. Wang, M.A. Meyers, Structure and mechanical behavior of human hair, Mater. Sci. Eng. C. 73 (2017) 152–163.
[14] G. Nikiforidis, C. Balas, D. Tsambaos, Viscoelastic response of human hair cortex, Med. Biol. Eng. Comput. 30 (1992) 83–88.
[15] H.A. Barnes, G.P. Roberts, The non-linear viscoelastic behaviour of human hair at moderate extensions, Int. J. Cosmet. Sci. 22 (2000) 259–264.
[16] M.S. Robinson, B.J. Rigby, Thiol differences along keratin fibers: stress/strain and stress-relaxation behavior as a function of temperature and extension, Text. Res. J. 55 (1985) 597–600.
[17] X. Xiao, J. Hu, D. Hui, Tensile-relaxation study of camel hair fi ber at elastic stretching region: analytical model and experiment, Compos. Part B 91 (2016) 559–568.
[18] M. Benzarti, M.B. Tkaya, C.P. Mattei, H. Zahouani, Hair mechanical properties depending on age and origin, World Acad. Sci. Eng. Technol. (2011) 471–477.

[19] L. Kreplak, J. Doucet, F. Briki, Unraveling double stranded α-helical coiled coils: an X-ray diffraction study on hard α-keratin fibers, Biopolymers. 58 (2001) 526–533.
[20] P. Mason, Thermal transitions in keratin part III stress and temperature effects in relation to the alpha beta transition, Text. Res. J. 35 (1965) 483–490.
[21] T. Motokawa, A. Tsuchi, Dynamic mechanical properties of body-wall dermis in various mechanical states and their implications for the behavior of sea cucumbers, Biol. Bull. 205 (2003) 261–275.
[22] G.K. Szulgit, R.E. Shadwick, Dynamic mechanical characterization of a mutable collagenous tissue: response of sea cucumber dermis to cell lysis and dermal extracts, J. Exp. Biol. 203 (2000) 1539–1550.
[23] O. Emile, A. Le Floch, F. Vollrath, Time-resolved torsional relaxation of spider draglines by an optical technique, Phys. Rev. Lett. 98 (2007) 1–4.
[24] L. Kreplak, J. Doucet, P. Dumas, F. Briki, New aspects of the α-helix to β-sheet transition in stretched hard α-keratin fibers, Biophys. J. 87 (2004) 640–647.
[25] M. Kania, D. Mikolajewska, K. Marycz, M. Kobielarz, Effect of diet on mechanical properties of horse's hair, Acta Bioeng. Biomech. 11 (2009) 53–57.
[26] J.B. Speakman, The plasticity of wool, Proc. R. Soc. B. 103 (1928) 377–396.
[27] L. Rebenfeld, H.D. Weigmann, C. Dansizer, Temperature dependence of the mechanical properties of human hair in relation to structure, J. Soc. Cosmet. Chem. 538 (1966) 525–538.
[28] A. Franbourg, P. Hallegot, F. Baltenneck, C. Toutain, F. Leroy, Current research on ethnic hair, J. Am. Acad. Dermatol. 48 (2003) S115–S119.
[29] I.P. Seshadri, B. Bhushan, Effect of ethnicity and treatments on in situ tensile response and morphological changes of human hair characterized by atomic force microscopy, Acta Mater. 56 (2008) 3585–3597.
[30] G. Wei, B. Bhushan, Nanotribological and nanomechanical characterization of human hair using a nanoscratch technique, Ultramicroscopy 106 (2006) 742–754.
[31] D.A. Greenberg, D.S. Fudge, Regulation of hard α-keratin mechanics via control of intermediate filament hydration: matrix squeeze revisited, Proc. R. Soc. B. 280 (2013) 1–8.
[32] S. Le Blond, E. Guilminot, G. Lemoine, N. Huet, J.Y. Mevellec, Vibrational Spectroscopy FT-Raman spectroscopy: a positive means of evaluating the impact of whale bone preservation treatment, Vib. Spectrosc. 51 (2009) 156–161.
[33] J.M. Gillespie, Keratin structure and changes with copper deficiency, Aust. J. Derm. 14 (1973) 127–132.
[34] Z.L. Shen, H. Kahn, R. Ballarini, S.J. Eppell, Viscoelastic properties of isolated collagen fibrils, Biophys. J. 100 (2011) 3008–3015.
[35] M. Zhan, R.P. Wool, Mechanical properties of chicken feather fibers, Polym. Compos. 32 (2011) 937–944.
[36] J. Jachowicz, Hair damage and attempts to its repair, J. Soc. Cosmet. Chem. 38 (1987) 263–286.
[37] C.R. Robbins, R.J. Crawford, Cuticle damage and the tensile properties of human hair, J. Soc. Cosmet. Chem. 42 (1991) 59–67.
[38] B. Wang, W. Yang, V.R. Sherman, M.A. Meyers, Pangolin armor: overlapping, structure, and mechanical properties of the keratinous scales, Acta Biomater. 41 (2016) 60–74.
[39] S.E. Naleway, M.M. Porter, J. Mckittrick, M.A. Meyers, Structural design elements in biological materials: application to bioinspiration, Adv. Mater. (2015) 5455–5476, https://doi.org/10.1002/adma.201502403.
[40] S. Kawabata, Y. Kawashima, Y. Yamashita, A. Tanaka, Apparent elastic modulus of scale estimated from bending property of single wool fiber, J. Text. Eng. 50 (2004) 21–24.
[41] B. Busson, F. Briki, J. Doucet, Side-chains configurations in coiled coils revealed by the 5.15-Å meridional reflection on hard α-Keratin X-Ray diffraction patterns, J. Struct. Biol. 125 (1999) 1–10.
[42] V.F. Monteiro, A.P. Maciel, E. Longo, Thermal analysis of caucasian human hair, J. Therm. Anal. Calorim. 79 (2005) 289–293.
[43] A. Idris, R. Vijayaraghavan, Usman Ali Rana, A.F. Patti, D.R. MacFarlane, Dissolution and regeneration of wool keratin in ionic liquids, Green Chem. 16 (2014) 2857–2864.
[44] E.S. El-Amoudy, E.M. Osman, Thermal stability and fastness properties of wool fabric dyed with an ecofriendly natural dye "sambucus nigra" under the effect of different mordants, Elixir Apllied Chem. 44C (2012) 7080–7085.
[45] W.T. Humphries, D.L. Miller, R.H. Wildnauer, The Thermomechanical analysis of natural and chemically modified human hair, J. Soc. Cosmet. Chem. 370 (1972) 359–370.
[46] S. Balaji, R. Kumar, R. Sripriya, U. Rao, A. Mandal, P. Kakkar, P.N. Reddy, P.K. Sehgal, Characterization of keratin-collagen 3D scaffold for biomedical applications, Polym. Adv. Technol. 23 (2012) 500–507.
[47] V. Signori, D.M. Lewis, FTIR investigation of the damage produced on human hair by weathering and bleaching processes: implementation of different sampling techniques and data processsing, Int. J. Cosmet. Sci. 19 (1997) 1–13.
[48] C.M. Carr, D.M. Lewis, An FTIR spectroscopic study of the photodegradation and thermal degradation of wool, J. Soc. Dye. Colour. 109 (1993) 21–24.
[49] B. Lipp-symonowicz, S. Sztajnowski, A. Kulak, IR spectroscopy as a possible method of analysing fibre structures and their changes under various impacts, Infrared Radiat. (2012) 27–40.
[50] C. Robbins, Chemical aspects of bleaching human hair, J. Soc. Cosmet. Chem. 22 (1971) 339–348.
[51] M. Feughelman, A two-phase structure for keratin fibers, Text. Res. J. 29 (1959) 223–228.
[52] M. Feughelman, Natural protein fibers, J. Appl. Polym. Sci. 83 (2002) 489–507.
[53] J.W.S. Hearle, A critical review of the structural mechanics of wool and hair fibres, Int. J. Biol. Macromol. 27 (2000) 123–138.
[54] C.M. Pande, FT-Raman spectroscopy–applications in hair research, J. Soc. Cosmet. Chem. 268 (1994) 257–268.
[55] M. Joy, D.M. Lewis, The use of Fourier transform infra-red spectroscopy in the study of the surface chemistry of hair fibres, Int. J. Cosmet. Sci. 13 (1991) 249–261.
[56] M. Feughelman, A model for the mechanical properties of the α-keratin cortex, Text. Res. J. 64 (1994) 236–239.
[57] L. Šimková, M. Skrontová, K. Jelen, B. Chalupa, Determination of different animal species hair viscoelastic properties, Trends in Agricultural Engineering, Czech University of Life Sciences, Prague590, 2013.